Electronic Supplementary Material (ESI) for Dalton Transactions

Supporting Information for

Reactivity comparison of high-valent iron(IV)-oxo complexes bearing *N*-tetramethylated cyclam ligands with different ring size

Seungwoo Hong,[a‡] Hee So,[a‡] Heejung Yoon,[a] Kyung-Bin Cho,[a] Yong-Min Lee,[a] Shunichi Fukuzumi*[ab] and Wonwoo Nam*[a]

[a] *Department of Bioinspired Science, Ewha Womans University, Seoul, 120-750, Korea.*

[b] *Department of Material and Life Science Graduate School of Engineering, Osaka University and ALCA (JST), 2-1 Yamada-oka, Suita, Osaka 565-0871, Japan.*

E-mail: fukuzumi@chem.eng.osaka-u.ac.jp, wwnam@ewha.ac.kr

Table of Contents

Experimental Section

Materials. All chemicals obtained from Aldrich Chemical Co. were the best available purity and used without further purification unless otherwise indicated. Solvents were dried according to published procedures and distilled under Ar prior to use.[1] Iodosylbenzene (PhIO) was prepared by a literature method.[2] $H_2{}^{18}O$ (95 % ^{18}O-enriched) was purchased from ICON Services Inc. (Summit, NJ, USA). 1,4,7,10-tetraazacyclotridecane was purchased from Chematech Co. (France). The deuterated substrate, xanthene-d_2, was prepared by taking xanthene (0.16 g, 0.87 mmol) in DMSO-d_6 (5.0 mL) along with NaH (0.10 g, 4.2 mmol) under an inert atmosphere.[3] The reaction solution was stirred for 8 h and quenched with D_2O (5.0 mL). The crude product was filtered and washed with copious amounts of H_2O. ^1H NMR confirmed >99% deuteration of xanthene. $Fe(CF_3SO_3)_2{\cdot}2CH_3CN$ was synthesized by reacting iron powder with trifluoromethanesulfonic acid (CF_3SO_3H) under an inert atmosphere in CH_3CN. 13-TMC ligand was prepared by reacting an excess amount of formaldehyde and formic acid with 1,4,7,10-tetraazacyclotridecane.[4] $[Fe^{IV}(O)(14\text{-TMC})(CH_3CN)]^{2+}$ (**1**) was prepared according to literature methods.[5]

Instrumentation. UV-vis spectra were recorded on a Hewlett Packard Agilent 8453 UV-visible spectrophotometer equipped with a circulating water bath or an UNISOKU cryostat system (USP-203; UNISOKU, Japan) or on a Hi-Tech Scientific (U.K.) SF-61 DX2 cryogenic stopped-flow spectrometer equipped with a Xe arc lamp and a KinetaScan diode array rapid scanning unit. Electrospray ionization mass (ESI-MS) spectra were collected on a Thermo Finnigan (San Jose, CA, USA) LCQ^{TM} Advantage MAX quadrupole ion trap instrument, by infusing samples directly into the source at 20 μL/min using a syringe pump. The spray voltage was set at 4.7 kV and the capillary temperature at 80 °C. CW-EPR spectra were taken at 5 K using an X-band Bruker EMX-plus spectrometer equipped with a dual mode cavity (ER 4116DM). Low temperatures were achieved and controlled with an Oxford Instruments ESR900 liquid He quartz cryostat with an Oxford Instruments ITC503 temperature and gas flow controller. The experimental parameters for EPR spectra were as follows: Microwave frequency = 9.646 GHz, microwave power = 1 mW, modulation amplitude = 10 G, gain = 1x 10^4, modulation frequency 100 kHz, Time constant = 40.96 ms, conversion time = 85.00 ms and measuring temperature = 5 K. ^1H NMR spectra were

measured with Bruker DPX-400 spectrometer. Resonance Raman spectra were obtained using a liquid nitrogen cooled CCD detector (CCD-1024x256-OPEN-1LS, HORIBA Jobin Yvon) attached to a 1-m single polychromator (MC-100DG, Ritsu Oyo Kogaku) with a 1200 grooves/mm holographic grating. Excitation wavelength of 407.0 nm was provided by He-Cd laser (Kimmon Koha, IK5651R-G and KR1801C), with 20 mW power at the sample point. All measurements were carried out with a spinning cell (1000 rpm) at –20 °C. Raman shifts were calibrated with indene, and the accuracy of the peak positions of the Raman bands was ±1 cm^{-1}. The isomer shifts were referenced against that of a room-temperature metallic iron foil. Analysis of the data was performed with the program WMOSS (WEB Research). Product analysis was performed with an Agilent Technologies 6890N gas chromatograph (GC) and Thermo Finnigan (Austin, Texas, USA) FOCUS DSQ (dual stage quadrupole) mass spectrometer interfaced with Finnigan FOCUS gas chromatograph (GC-MS).

Synthesis of $[Fe^{II}(13\text{-TMC})(CF_3SO_3)](CF_3SO_3)$. Iron(II) complex, $[Fe^{II}(13\text{-TMC})(CH_3CN)]^{2+}$ was prepared by mixing $Fe(CF_3SO_3)_2{\cdot}2CH_3CN$ (0.60 g, 1.2 mmol) and 13-TMC (0.20 g, 0.83 mmol) in CH_3CN (2.0 mL). The mixture was stirred for 12 h, and then diethyl ether (10 mL) was added to the resulting solution to yield white powder, which was collected by filtration, washed with diethyl ether, and dried in vacuo. Yield: 0.30 g (80 %). ESI-MS in acetonitrile: *m/z* of 169.5 for $[Fe^{II}(13\text{-TMC})(NCCH_3)]^{2+}$ and *m/z* of 447.2 for $[Fe^{II}(13\text{-TMC})(CF_3SO_3)]^{+}$ (ESI,† Fig. S1). *Anal.* Calc. for $C_{15}H_{30}F_6FeN_4O_6S_2$: C, 30.21; H, 5.07; N, 9.39. Found: C, 30.42; H, 5.02; N, 9.27%.

Generation and Characterization of $[Fe^{IV}(O)(13\text{-TMC})]^{2+}$ (2). PhIO (0.75 mM, 1.5 equiv.) was added to acetonitrile solution containing $[Fe^{II}(13\text{-TMC})(CF_3SO_3)](CF_3SO_3)$ (0.50 mM) at –40 °C, producing a green solution (λ_{max} = 735 nm, ε = 240 M^{-1} cm^{-1}). Resonance Raman (rRaman) and ESI-MS spectroscopic measurements were performed for the characterization of **2**. The ^{18}O-labeled iron(IV)-oxo complex, $[Fe^{IV}(^{18}O)(13\text{-TMC})]^{2+}$ (**2**-^{18}O), was prepared by reacting $[Fe^{II}(13\text{-TMC})(CF_3SO_3)](CF_3SO_3)$ (0.50 mM) and PhIO (0.75 mM) in the presence of $H_2{}^{18}O$ (10 μL) in CH_3CN at –40 °C. Upon excitation at 407 nm, the isotopic shifts of resonance-enhanced vibrations were observed (833 cm^{-1} for **2**-^{16}O and 797 cm^{-1} for **2**-^{18}O).

In ESI-MS (in CH_3CN), m/z = 463.0 for $[Fe^{IV}(^{16}O)(13\text{-TMC})(CF_3SO_3)]^+$ and m/z = 465.1 for $[Fe^{IV}(^{18}O)(13\text{-TMC})(CF_3SO_3)]^+$ were observed (Fig. 1).

Spectral Redox Titration. Redox titration of electron-transfer from bromoferrocene (BrFc) to $[Fe^{IV}(O)(13\text{-TMC})]^{2+}$ (0.50 mM) was examined using different concentrations of BrFc (0.10 – 2.5 mM) in CH_3CN at –40 °C. The concentration of bromoferricenium ion ($BrFc^+$) was determined from the absorption band at 570 nm because of the overlap of absorption band λ = 675 nm due to $BrFc^+$ (ε_{BrFc+} = 320 M^{-1} cm^{-1}) and λ = 735 nm due to $[Fe^{IV}(O)(13\text{-TMC})]^{2+}$ (ε_{FeIV} = 240 M^{-1} cm^{-1}). The concentration of $BrFc^+$ produced was then calculated by eqn (S2), which was derived from eqn (S1). $\{[Fe^{IV}(O)(13\text{-TMC})]^{2+}\}_0$ in eqn (2) denotes the initial concentration of $[Fe^{IV}(O)(13\text{-TMC})]^{2+}$.

$$Abs_{570} = \varepsilon_{BrFc+}[Br_2Fc^+] + \varepsilon_{FeIV}\{[Fe^{IV}(O)(13\text{-TMC})]^{2+}\} \quad (S1)$$

$$[BrFc^+] = (Abs_{570} - \varepsilon_{FeIV}\{[Fe^{IV}(O)(13\text{-TMC})]^{2+}\}_0)/(\varepsilon_{BrFc+} - \varepsilon_{FeIV}) \quad (S2)$$

The ε value of $BrFc^+$ was confirmed by carrying out an electron-transfer oxidation of BrFc by cerium(IV) ammonium nitrate in CH_3CN at –40 °C.

Reactivity Studies. All reactions were run in a 1-cm UV cuvette and followed by monitoring UV-vis spectral changes of reaction solutions, and rate constants were determined by fitting the changes in absorbance at 820 nm for $[Fe^{IV}(O)(14\text{-TMC})(CH_3CN)]^{2+}$ (**1**) and at 735 nm for $[Fe^{IV}(O)(13\text{-TMC})]^{2+}$ (**2**). The intermediate **2** (0.50 mM) was used in C-H bond activation reactions of various substrates with different bond dissociation energy (BDE), such as 10-methyl-9,10-dihydroacridine ($AcrH_2$, 73.7 kcal mol^{-1}), xanthene (75.5 kcal mol^{-1}), 9,10-dihydroanthracene (DHA, 77 kcal mol^{-1}), and 1,4-cyclohexadiene (CHD, 78 kcal mol^{-1}) and in OAT reaction of thioanisole in CH_3CN at –40 °C. Given that the second-order rate constants (k_2) of C-H bond activation and OAT reactions for **1** have already been determined in CH_3CN at 25 °C and 15 °C,[6,7] respectively, temperature-dependent kinetic experiments were performed with **1** (0.50 mM) in order to estimate its k_2 in CH_3CN at –40 °C. The kinetic isotope effect value (KIE) of the reaction between **2** and xanthene was determined by

comparing k_2 values obtained from C-H bond activation reactions of xanthene and that of xanthene-d_2 in CH_3CN at –40 °C. Reactions were run at least in triplicate, and the data reported represent the average of these reactions.

For product analysis, the purity of substrates was checked with GC and GC-MS prior to use. Products were identified by comparing with authentic samples, and product yields were determined by comparison against standard curves prepared with authentic samples and using decane as an internal standard.

References

1. W. L. F. Armarego and C. L. L. Chai, *Purification of Laboratory Chemicals*, 6th edn, Pergamon Press, Oxford, U.K, 2009.
2. H. Saltzman and J. G. Sharefkin, *Organic Syntheses*, Wiley, New York, 1973, Collect. Vol. V, pp. 658.
3. C. R. Goldsmith, R. T. Jonas and T. D. P. Stack, *J. Am. Chem. Soc.,* 2002, **124**, 83.
4. J. A. Halfen and V. G. Young, Jr., *Chem. Commun*., 2003, 2894.
5. J.-U. Rohde, J. In, M. H. Lim, W. W. Brennessel, M. R. Bukowski, A. Stubna, E. Münck, W. Nam and L. Que, J., *Science.,* 2003, **299**, 1037.
6. C. V. Sastri, J. Lee, K. Oh, Y. J. Lee, J. Lee, T. A. Jackson, K. Ray, H. Hirao, W. Shin, J. A. Halfen, J. Kim, L. Que, J., S. Shaik and Nam, W. *Proc. Natl. Acad. Sci. USA.,* 2007, **104**, 19183.
7. S. A. Wilson, J. Chen, S. Hong, Y.-M. Lee, M. Clémancey, R. Garcia-Serres, T. Nomura, T. Ogura, J.-M. Latour, B. Hedman, K. O. Hodgson, W. Nam and E. I. Solomon, *J. Am. Chem. Soc*., 2012, **134**, 11791.

Table S1. Second-order rate constants (k_2) and apparent second-order rate constants (k_2') determined in substrate oxidations (e.g., C–H bond activation and oxygen atom transfer reactions) by $[Fe^{IV}(O)(14\text{-TMC})(CH_3CN)]^{2+}$ (**1**) and $[Fe^{IV}(O)(13\text{-TMC})]^{2+}$ (**2**) in CH_3CN at -40 °C.

			1		**2**	
	Substrate	C-H BDE,[a] kcal/mol	k_2, $M^{-1}\,s^{-1}$	k_2',[b] $M^{-1}\,s^{-1}$	k_2, $M^{-1}\,s^{-1}$	k_2',[b] $M^{-1}\,s^{-1}$
C-H activation	$AcrH_2$	73.7	1.0	5.0×10^{-1}	540	270
	Xanthene	75.5	6.6×10^{-2}	3.3×10^{-2}	18	9
	DHA	77	2.5×10^{-3}	6.3×10^{-4}	5.7	1.4
	CHD	78	6.4×10^{-4}	1.6×10^{-4}	5.4	1.3
	Fluorene	80	3.2×10^{-5}	1.6×10^{-5}		
OAT	Thioanisole		1.3×10^{-3}		430	

[a] See references: (*a*) T. Matsumoto, K. Okubo, K. Honda, A. Yazawa, H. Furutachi, S. Fujinami, S. Fukuzumi and M. Suzuki, *J. Am. Chem. Soc,* 2009, **131**, 9258; (*b*) Y.-R. Luo, *Handbook of bond dissociation energies in organic compounds*, CRC Press, New York, 2003.

[b] All k_2 values in C–H bond activation reactions were adjusted for reaction stoichiometry to yield k_2' values based on the number of equivalent target C–H bonds in the substrate (e.g., two for xanthene and four for DHA)

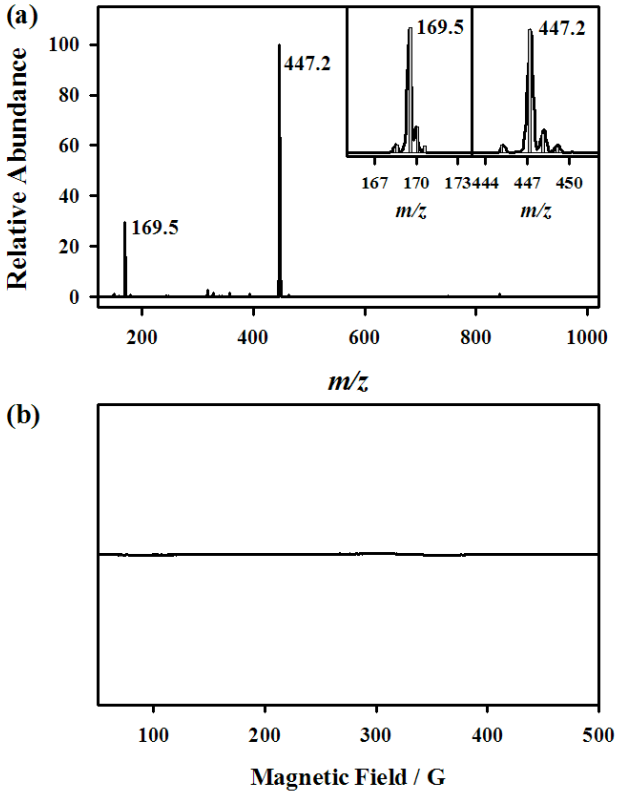

Figure S1. (a) ESI-MS spectrum of $[Fe^{II}(13\text{-TMC})]^{2+}$. Mass and isotope distribution patterns of two prominent ion peaks at *m/z* 169.5 and 447.2 correspond to $[Fe^{II}(13\text{-TMC})(CH_3CN)]^{2+}$ (*calcd. m/z* 169.6) and $[Fe^{II}(13\text{-TMC})(CF_3SO_3)]^{+}$ (*caldc. m/z* 447.1), respectively. Inset shows the isotopic distribution patterns of each peak. (b) X-band EPR spectrum of $[Fe^{II}(13\text{-TMC})]^{2+}$ (1.0 mM) measured at 5 K.

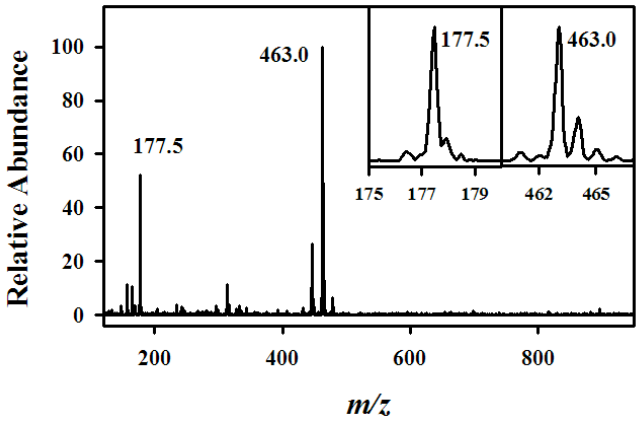

Figure S2. (a) ESI-MS spectrum of $[Fe^{IV}(O)(13\text{-TMC})]^{2+}$. Mass and isotope distribution patterns of two prominent ion peaks at *m/z* 177.5 and 463.0 correspond to $[Fe^{IV}(O)13\text{-TMC})(CH_3CN)]^{2+}$ (*calcd. m/z* 177.6) and $[Fe^{IV}(O)(13\text{-TMC})(CF_3SO_3)]^{+}$ (*calcd. m/z* 463.1), respectively. Inset shows the isotopic distribution patterns of each peak.

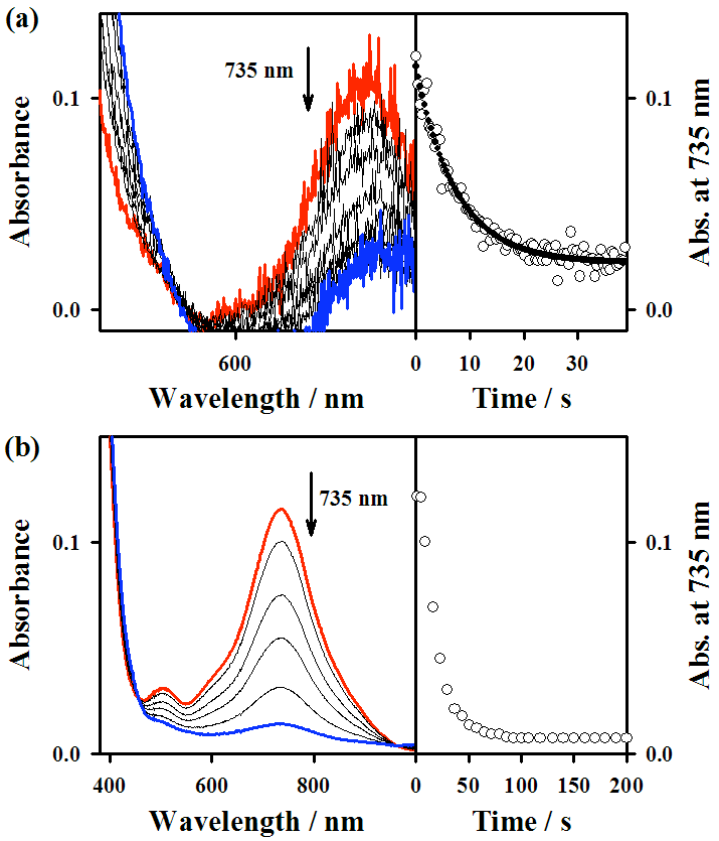

Figure S3. (a) UV-vis spectral changes observed in the reaction of **2** (0.50 mM) and xanthene (5.0 mM) in CH_3CN at –40 °C (left panel) and time course of the absorbance monitored at 735 nm due to **2** (right panel). (b) UV-vis spectral changes observed in the reaction of **2** (0.50 mM) and CHD (10 mM) in CH_3CN at –40 °C (left panel) and time course of the absorbance monitored at 735 nm due to **2** (right panel).

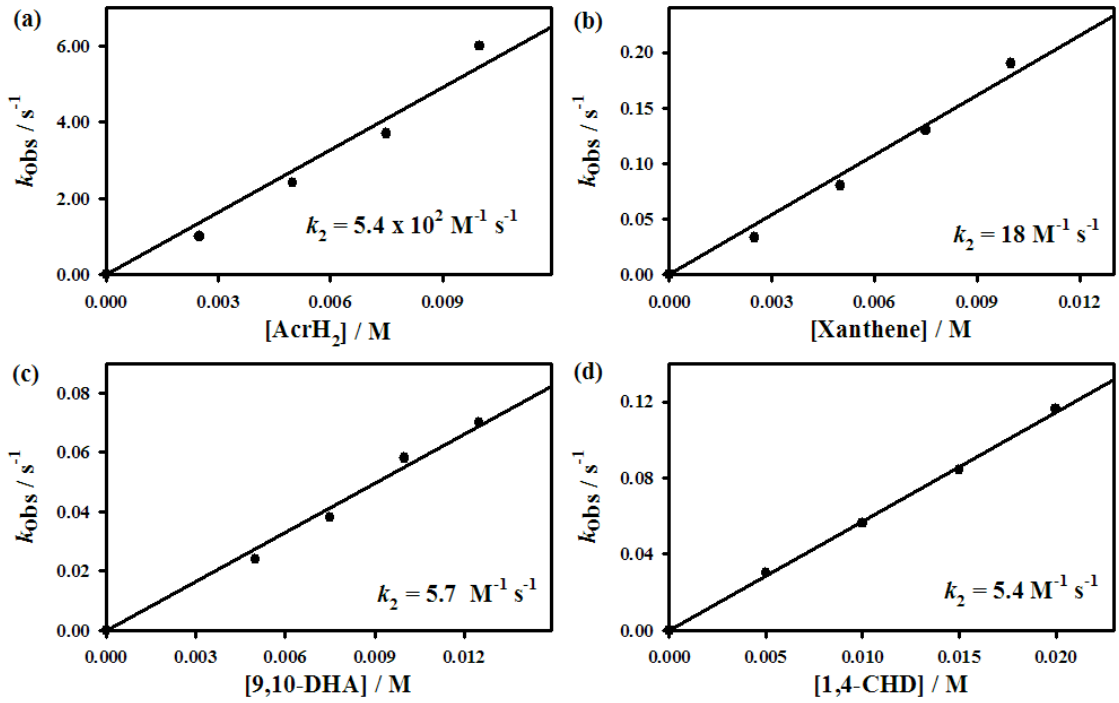

Figure S4. Plots of pseudo-first-order rate constants (k_{obs}) against the concentration of substrates ((a) $AcrH_2$, (b) xanthene, (c) DHA, and (d) CHD) to determine second-order rate constants (k_2) in the C–H bond activation reaction of substrates by **2** in CH_3CN at –40 °C (see Table S1).

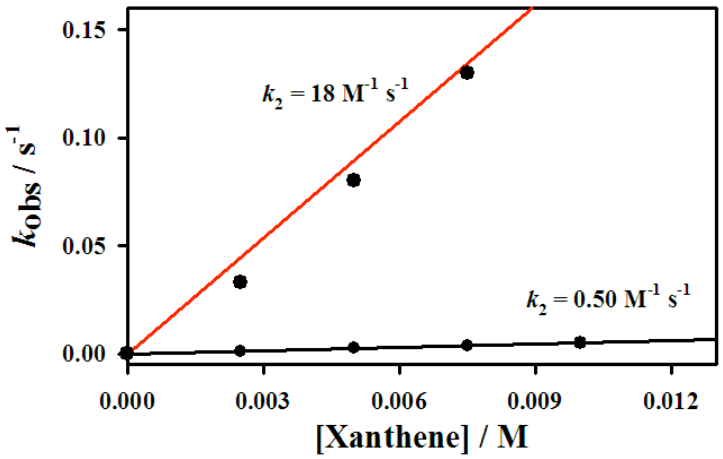

Figure S5. Plots of pseudo-first-order rate constants (k_{obs}) against the concentration of xanthene (red line) and xanthene-d_2 (black line) to determine second-order rate constants (k_2) in the oxidation of xanthene and xanthene-d_2 by **2** in CH_3CN at –40 °C. KIE value was determined to be 36.

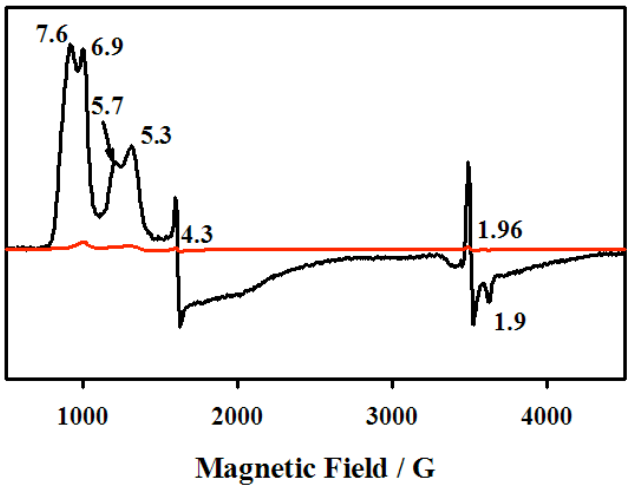

Figure S6. X-band CW-EPR spectra of the resulting solutions obtained in the reaction of **2** (1.0 mM) with cyclohexadiene (5.0 mM) (black line) and after addition of dimethylferrocene (Me_2Fc, 5.0 mM, red line) in CH_3CN at –40 ^{o}C. EPR spectra were measured at 5 K.

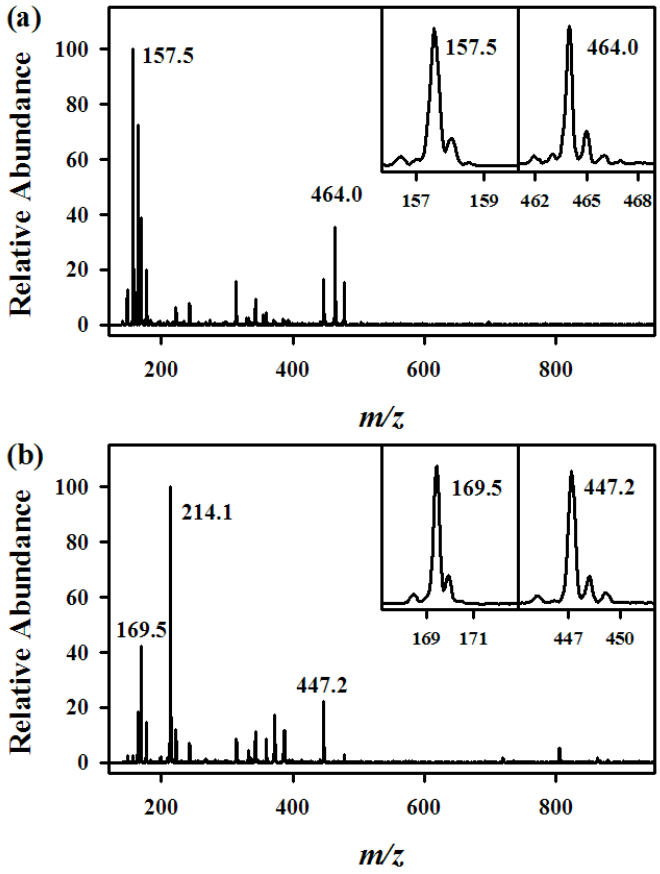

Figure S7. (a) ESI-MS spectrum of the reaction solution of $[Fe^{IV}(O)(13\text{-TMC})]^{2+}$ (1.0 mM) and cyclohexadiene (5.0 mM). Two prominent ion peaks at *m/z* 157.5 and 464.0 correspond to $[Fe^{III}(OH)(13\text{-TMC})]^{2+}$ (*calcd. m/z* 157.6) and $[Fe^{III}(OH)(13\text{-TMC})(CF_3SO_3)]^{+}$ (*calcd. m/z* 464.1), respectively. Inset shows the isotopic distribution patterns of each peak. (b) ESI-MS spectrum taken after addition of Me_2Fc (5.0 mM) to the reaction solution of $[Fe^{IV}(O)(13\text{-TMC})]^{2+}$ (1.0 mM) and cyclohexadiene (5.0 mM). Two prominent ion peaks at *m/z* 169.5 and 447.2 correspond to $[Fe^{II}(13\text{-TMC})(NCCH_3)]^{2+}$ (*calcd. m/z* 169.6) and $[Fe^{II}(13\text{-TMC})(CF_3SO_3)]^{+}$ (*calcd. m/z* 447.1), respectively. Inset shows the isotopic distribution patterns of each peak. The peak at *m/z* 214.1 corresponds to Me_2Fc^{+} (*calcd. m/z* 214.1).

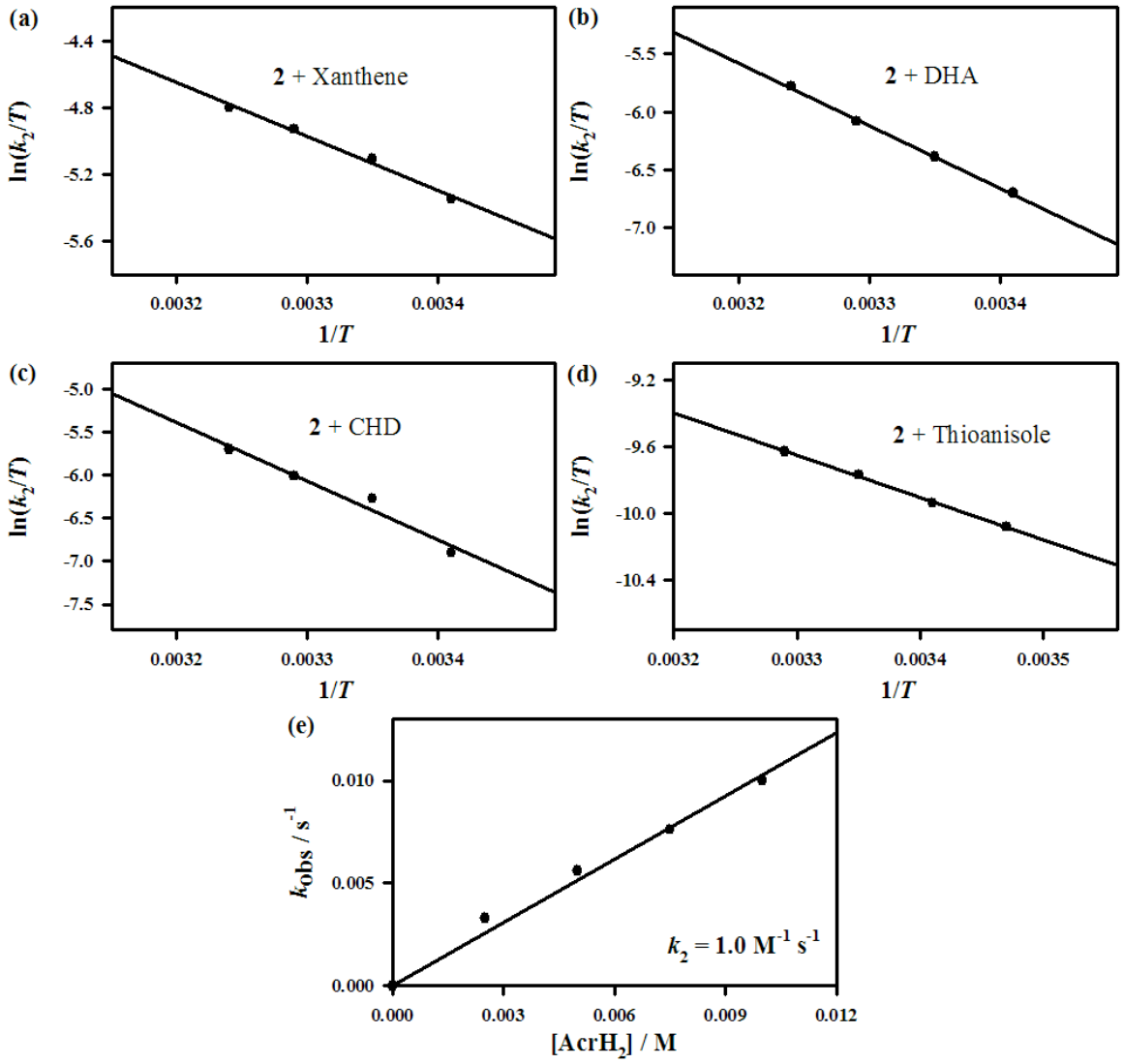

Figure S8. Eyring plots of ln(k_2/T) against $1/T$ in the reactions of **1** with (a) xanthene, (b) DHA, (c) CHD and (d) thioanisole to estimate second-order rate constants in CH_3CN at -40 °C. (e) Plots of pseudo-first-order rate constants (k_{obs}) against $AcrH_2$ concentration in the reaction of $AcrH_2$ by **1** in CH_3CN at -40 °C (see Table S1).

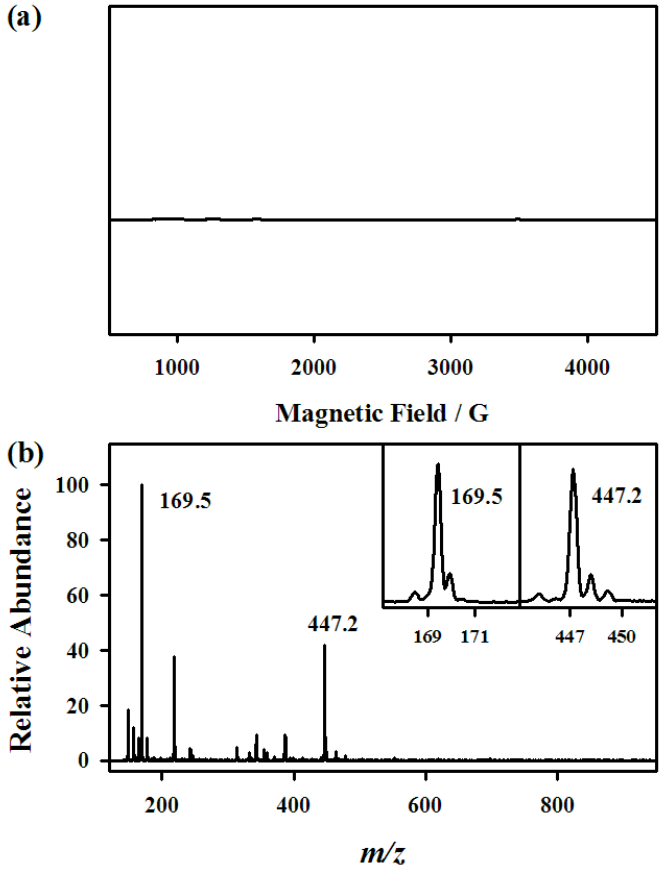

Figure S9. (a) X-band EPR spectrum of the reaction solution of $[Fe^{IV}(O)(13\text{-TMC})]^{2+}$ (**2**) (1.0 mM) and thioanisole (5.0 mM) in CH_3CN at –40 °C. EPR spectrum was recorded at 5 K. (b) ESI-MS spectrum of the reaction solution of **2** (1.0 mM) and thioanisole (5.0 mM) in CH_3CN at -40 °C. Two prominent ion peaks at *m/z* 169.5 and 447.2 correspond to $[Fe^{II}(13\text{-TMC})(NCCH_3)]^{2+}$ (*calcd. m/z* 169.6) and $[Fe^{II}(13\text{-TMC})(CF_3SO_3)]^{+}$ (*calcd. m/z* 447.1), respectively. Inset shows the isotopic distribution patterns of each peak.

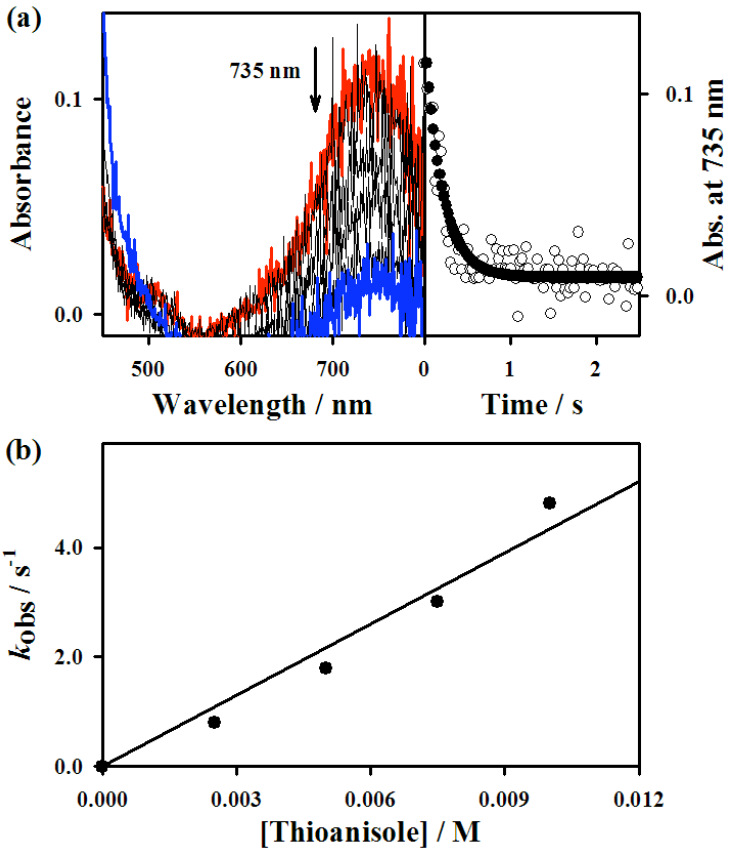

Figure S10. (a) UV-vis spectral changes observed in the reaction of **2** (0.50 mM) and thioanisole (5.0 mM) in CH_3CN at –40 °C (left panel) and time course of the absorbance monitored at 735 nm due to **2** (right panel). (b) Plots of pseudo-first-order rate constants (k_{obs}) against thioanisole concentration to determine the second-order rate constant in CH_3CN at –40 °C (see Table S1).

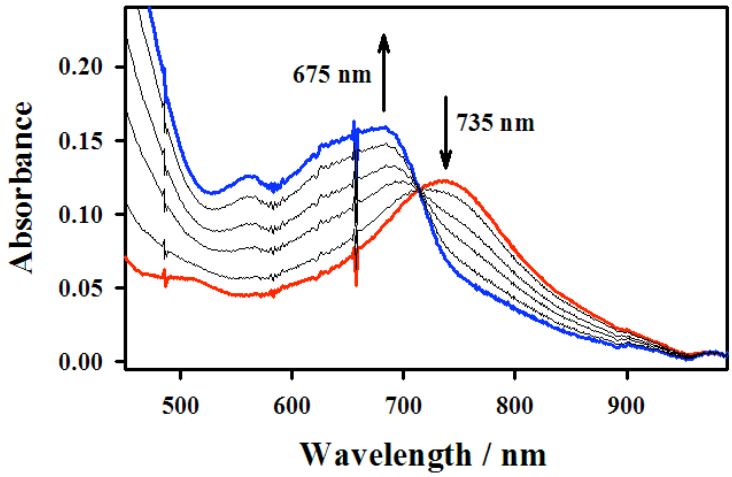

Figure S11. UV-vis spectral changes observed in the electron transfer from BrFc (5.0 mM) to **2** (0.50 mM) in CH_3CN at –40 °C.

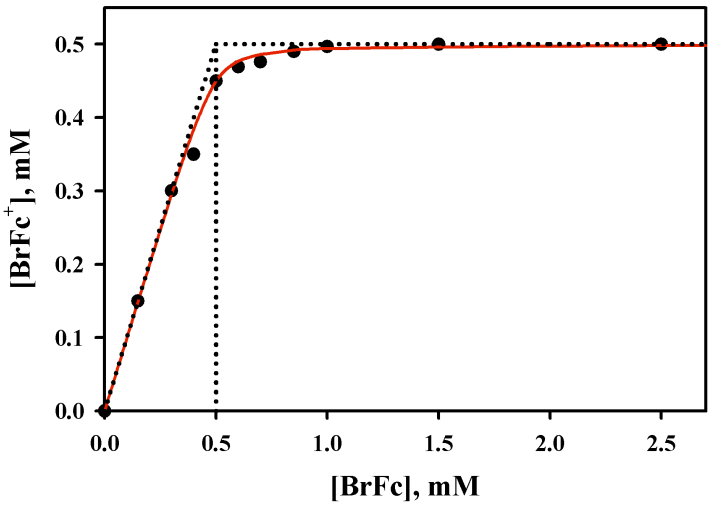

Figure S12. Plot of concentration of $BrFc^+$ produced in electron transfer from BrFc (0.54 V *vs.* SCE) to **2** against initial concentration of BrFc, $[BrFc]_0$, in CH_3CN at –40 °C. The equilibrium constant was determined to be 28.

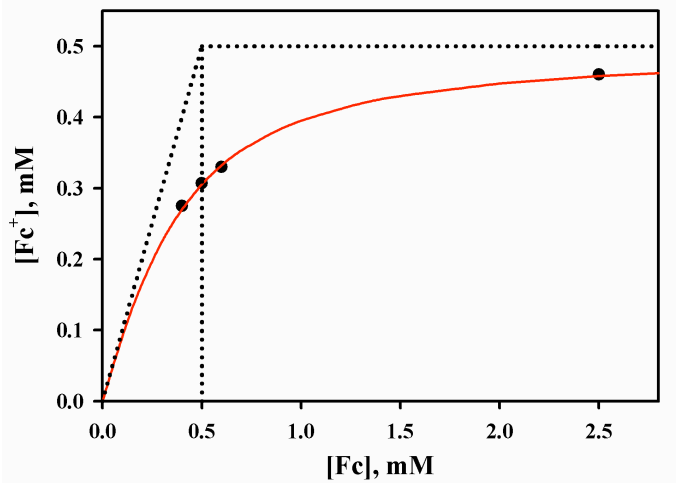

Figure S13. Plot of concentration of Fc^+ produced in electron transfer from Fc (0.37 V *vs.* SCE) to **1** against initial concentration of Fc, $[Fc]_0$, in CH_3CN at –40 °C. The equilibrium constant was determined to be 2.5.

DFT Calculation Section

DFT Calculation Methods. Density functional theory (DFT)[8] was applied at B3LYP/LACV3P^{*+}//B3LYP/LACVP level[9] using Gaussian 09.[10] The high molecular charge (2+) made it necessary to perform the optimizations in solvent to avoid artificial results.[11] The solvent (acetonitrile) effects were included using CPCM model with UFF cavity, per G09 default.[12] Dispersion was included using DFT-D3 program.[13]

References

8. W. Kohn and L. J. Sham, *Phys. Rev.*, 1965, **140**, A1133-A1138.
9. (a) A. D. Becke, *Phys. Rev. A*, 1988, **38**, 3098; (b) A. D. Becke, *J. Chem. Phys.*, 1993, **98**, 1372-1377; (c) A. D. Becke, *J. Chem. Phys.*, 1993, **98**, 5648-5652; (d) C. Lee, W. Yang and R. G. Parr, *Phys. Rev. B*, 1988, **37**, 785-789; e) P. J. Hay and W. R. Wadt, *J. Chem. Phys.*, 1985, **82**, 299-310.
10. M. J. Frisch, G. W. Trucks, H. B. Schlegel, G. E. Scuseria, M. A. Robb, J. R. Cheeseman, G. Scalmani, V. Barone, B. Mennucci, G. A. Petersson, H. Nakatsuji, M. Caricato, X. Li, H. P. Hratchian, A. F. Izmaylov, J. Bloino, G. Zheng, J. L. Sonnenberg, M. Hada, M. Ehara, K. Toyota, R. Fukuda, J. Hasegawa, M. Ishida, T. Nakajima, Y. Honda, O. Kitao, H. Nakai, T. Vreven, J. A. Montgomery, J. E. Peralta, F. Ogliaro, M. Bearpark, J. J. Heyd, E. Brothers, K. N. Kudin, V. N. Staroverov, R. Kobayashi, J. Normand, K. Raghavachari, A. Rendell, J. C. Burant, S. S. Iyengar, J. Tomasi, M. Cossi, N. Rega, J. M. Millam, M. Klene, J. E. Knox, J. B. Cross, V. Bakken, C. Adamo, J. Jaramillo, R. Gomperts, R. E. Stratmann, O. Yazyev, A. J. Austin, R. Cammi, C. Pomelli, J. W. Ochterski, R. L. Martin, K. Morokuma, V. G. Zakrzewski, G. A. Voth, P. Salvador, J. J. Dannenberg, S. Dapprich, A. D. Daniels, Farkas, J. B. Foresman, J. V. Ortiz, J. Cioslowski and D. J. Fox, *Gaussian Inc.*, Wallingford CT, 2009.
11. A. J. Johansson, M. R. A. Blomberg and P. E. M. Siegbahn, *J. Chem. Phys.*, 2008, **129**, 154301-154313.
12. (a) M. Cossi, N. Rega, G. Scalmani and V. Barone, *J. Comput. Chem.*, 2003, **24**, 669-681; (b) V. Barone and M. Cossi, *J. Phys. Chem. A*, 1998, **102**, 1995-2001.
13. S. Grimme, J. Antony, S. Ehrlich and H. Krieg, *J. Chem. Phys.*, 2010, **132**, 154104.

Table S2. $[Fe^{IV}(O)(13\text{-TMC})]^{2+}$ in kcal/mol.

	Δlacvp	Δlacv3p^{*+}	ΔZ_0	**ΔE**[a]	$\Delta E_{Thermal}$[b]	-TΔS[b]	ΔDispersion	**ΔG**[c]
$^3[Fe^{IV}(O)(13\text{-TMC})]^{2+}$	0.00	+0.00	+0.00	**0.00**	+0.00	+0.00	+0.00	**0.00**
$^5[Fe^{IV}(O)(13\text{-TMC})]^{2+}$	11.55	-3.03	-1.75	**6.77**	0.57	-1.79	1.84	**7.39**

[a] Sum of the previous three columns. [b] T = 298.15 K. [c] ΔG=Sum of the previous four columns.

Table S3. Mulliken spin density distribution for $[Fe^{IV}(O)(13\text{-TMC})]^{2+}$.

	Fe	O	4 x ligated N	Rest
$^3[Fe^{IV}(O)(13\text{-TMC})]^{2+}$	1.35	0.75	-0.09	-0.02
$^5[Fe^{IV}(O)(13\text{-TMC})]^{2+}$	3.21	0.54	0.29	0.06

Table S4. Selected $[Fe^{IV}(O)(13\text{-TMC})]^{2+}$ distances (Å).

	D(Fe-O)	D(Fe-N_{eq1})	D(Fe-N_{eq2})	D(Fe-N_{eq3})	D(Fe-N_{eq4})
$^3[Fe^{IV}(O)(13\text{-TMC})]^{2+}$	1.62	2.05	2.07	2.07	2.03
$^5[Fe^{IV}(O)(13\text{-TMC})]^{2+}$	1.64	2.12	2.18	2.09	2.20

Coordinates

Coordinates are in xyz-format with charge/multiplicity in parenthesis.

```
49
Low spin (2/3)
Fe -0.03252 -1.99568 2.33064
N 2.00838 -2.05718 2.56107
N 0.26706 -0.27940 1.20906
N -2.08411 -1.81812 2.51435
N -0.09363 -3.21476 3.95452
C -0.11881 -0.39615 -0.24273
C 1.76360 0.02624 1.27455
C 2.38198 -0.59166 2.51501
C 2.72440 -2.82639 1.47999
O -0.10921 -3.09432 1.14496
C -0.47759 0.87240 1.87234
C -1.98653 0.69198 2.02169
C -2.41685 -0.41211 2.98582
C -2.86046 -2.16248 1.26961
C 1.07545 -2.72065 4.78048
C 2.32496 -2.68382 3.91360
C 0.03553 -4.67851 3.63378
C -1.41027 -2.93327 4.64339
C -2.48645 -2.82733 3.58314
H 0.07596 -5.24703 4.56850
H -0.81948 -4.99852 3.04182
H 0.93714 -4.85930 3.05426
H -2.55918 -3.15241 0.93201
H -3.93163 -2.15091 1.49896
H -2.66267 -1.44761 0.47817
H 0.19542 0.50918 -0.77308
H 0.36975 -1.26956 -0.67148
H -1.19336 -0.50901 -0.34846
H 1.91087 1.11044 1.26643
H 2.22423 -0.36826 0.36913
H 2.48904 -2.41986 0.50011
H 3.80454 -2.76952 1.65314
H 2.39872 -3.86426 1.50443
H 2.00658 -0.12087 3.42869
H 3.47216 -0.48246 2.50321
H 3.11914 -2.11608 4.40701
H 2.70815 -3.68832 3.73352
H -1.63894 -3.73218 5.35639
H -1.30776 -2.00366 5.20793
H -3.44511 -2.53103 4.02200
H -2.63331 -3.78497 3.08177
H -1.93713 -0.26288 3.95823
H -3.50168 -0.36660 3.14202
H -2.36824 1.63345 2.43538
H -2.47570 0.58764 1.04925
H -0.02420 1.02882 2.85716
H -0.27411 1.76822 1.27283
H 0.82305 -1.72268 5.15180
H 1.22156 -3.37142 5.64997
49
High spin (2/5)
Fe -0.07538 -2.05650 2.19709
N 2.02601 -2.10212 2.50285
N 0.29802 -0.16099 1.19253
N -2.13406 -1.87359 2.47682
N -0.09051 -3.24617 4.05046
C -0.05992 -0.25197 -0.26776
C 1.78946 0.09584 1.32458
C 2.37731 -0.62526 2.53078
C 2.77029 -2.82420 1.41303
O -0.15133 -3.22170 1.04382
C -0.48939 0.93986 1.87482
C -1.99479 0.67336 1.97236
C -2.41853 -0.44537 2.92889
C -2.94020 -2.23690 1.25935
C 1.11138 -2.72652 4.77990
C 2.32130 -2.75646 3.84709
C 0.00155 -4.72121 3.79426
C -1.40360 -2.88393 4.68194
C -2.48494 -2.83843 3.60513
H 0.05590 -5.25685 4.74949
H -0.87260 -5.05616 3.23858
H 0.88279 -4.95003 3.19824
H -2.68005 -3.24945 0.95454
H -4.00727 -2.17827 1.49855
H -2.72077 -1.55487 0.44143
H 0.19299 0.68824 -0.77138
H 0.49121 -1.07363 -0.72389
H -1.12393 -0.44102 -0.39029
H 1.97222 1.17219 1.41166
H 2.26867 -0.23510 0.40226
H 2.57293 -2.36257 0.44785
H 3.84565 -2.78960 1.61998
H 2.43230 -3.85883 1.37803
H 1.98714 -0.20892 3.46441
H 3.46792 -0.51645 2.54603
H 3.17029 -2.24643 4.31375
H 2.62972 -3.78260 3.64619
H -1.68059 -3.61785 5.44787
H -1.28927 -1.91811 5.17945
H -3.44422 -2.53472 4.03853
H -2.62236 -3.82026 3.15037
H -1.92945 -0.30417 3.89682
H -3.50130 -0.38743 3.09709
H -2.44349 1.59105 2.37218
H -2.44430 0.54660 0.98320
H -0.06853 1.06945 2.87717
H -0.31707 1.86978 1.31725
H 0.89089 -1.70674 5.10943
H 1.32063 -3.32785 5.67
```